Pressure Sensor Devices Featuring a Chemical Passivation Made of a Locally Synthesized Diamond Layer

Mario Bähr,* Indira Käpplinger, Paulius Pobedinskas, Thomas Frank, André Grün, Ken Haenen, and Thomas Ortlepp

The rear side of a pressure sensor diaphragm is prepared with an additional diamond layer as protective coating against harsh media. The preparation sequence for the diamond coating is developed as a simple backend process, combining only two additional steps in the standard process. These are the local seeding of nanodiamond layer and the low-temperature diamond growth at <300 °C in a linear antenna microwave plasma-enhanced chemical vapor deposition reactor, where only at the nanodiamond seeded sites, a high-quality diamond film was synthesized. The seeding resolution in the setup used was limited to ≈80 μm, but can be further reduced. In an industry-typical assembly sequence the diamond coated pressure sensor devices are further equipped with a support wafer and mounted to a TO-8 socket. Tests of such sensor systems indicate that the diamond layer does not hamper the stability of the device. This proofed method of postprocessing an only-local and low-temperature synthesis of a diamond layer on the wafer-level opens- up possibilities for many other applications, since this approach is scalable and in general cost effective.

1. Introduction

In modern industries, piezoresistive mechanical sensors are the key technology. In many industrial processes, pressure must be controlled with a high accuracy. Special challenges arise for microelectromechanical system (MEMS) sensor devices when they are used in harsh environments, which can be characterized by high temperatures, large temperature changes, or corrosive media. These conditions can lead to a degradation and thus to instabilities or large tolerances in the measurement signals or even a total failure. For example, pressure or flow measurements in aggressive media: if sensor components are directly exposed to the measured medium, it must not have a corrosive effect on them. Otherwise, there is a risk of damaging the sensor. To avoid this, the sensor can be protected with additional passivating layers such as silicon dioxide and/or silicon nitride, or parylene,[1,2] or use an additional membrane and pressure-transmitting medium.

Passivation layers are preferred; however, they are not always resistant to all media. For example, due to the harsh environment, pressure sensors with SiO_2 passivation layer experience premature aging and therefore a regular and frequent replacement of the sensors after certain intervals is needed.

Synthetic diamond due to its chemical inertness and resistance has the potential to be a perfect passivating material. Hence, our aim is to proof, first, an industrially feasible technological route of implementing a low-temperature growth of a ≈500 nm thick diamond layer on a sensor device. Second, to show that the sensor is capable to withstand an industry-type test regime of being used in harsh media.

In present industrial applications, nanocrystalline diamond (NCD) is used as a mechanically highly stable and reliable material, e.g., in clockworks, as surgery instruments and also MEMS devices.[3–5] Deposition of diamond by means of chemical vapor deposition technologies (CVD) on blank or coated silicon wafers is widely used,[3,4,6,7] whereas the low-temperature deposition of diamond films at temperatures <400 °C is challenging.[8–10] In previous work, also diamond-based pressure sensors were discussed, using either a diamond diaphragm in rigid diamond[11,12] or thin layers of diamond on glass.[13,14] All making use of the piezoresistive effects in doped diamond films.[15] The use of diamond and diamond-like carbon layers as corrosion-resistant passivation layers was also studied in the past, concluding that for many applications, nano- and microcrystalline diamond provides a superior chemical resistance against corrosive agents.[16–18]

Despite of all the positive properties, the synthetic diamond layers are not yet available in industrial MEMS devices based on CMOS-compatible manufacturing, which comes due to the

M. Bähr, I. Käpplinger, T. Frank, A. Grün, T. Ortlepp
CiS Forschungsinstitut für Mikrosensorik GmbH
Konrad-Zuse-Str. 14, 99099 Erfurt, Germany
E-mail: mbaehr@cismst.de

P. Pobedinskas, K. Haenen
Institute for Materials Research (IMO)
Hasselt University
Wetenschapspark 1, 3590 Diepenbeek, Belgium

P. Pobedinskas, K. Haenen
IMOMEC
IMEC vzw
Wetenschapspark 1, 3590 Diepenbeek, Belgium

most probable reason of an incompatible process technology: typically, diamond layers are synthesized at the temperatures of 600–800 °C, and the diamond layers can only be patterned using an inductively coupled reactive ion plasma etching (IC-RIE) that requires a hard mask. Thus, the implementation of diamond layer processing is challenging. To overcome the drawbacks of CMOS processing incompatibilities, we suggest a low-temperature diamond deposition[9] only at those sites of a sensor devices that are exposed to a corrosive environment. This idea requires a highly localized diamond synthesis at temperatures below 300 °C, performed as back-end process. In this contribution, both issues, the techniques to perform the local diamond synthesis and the low-temperature diamond, are addressed. The localized growth makes the patterning of diamond by IC-RIE no longer necessary, and the low temperature is compatible to relevant metallization schemes of the sensor device, e.g., AlSi. The local synthesis of diamond using local seeding or selective nucleation was introduced several years ago by means of different approaches.[4,19,20]. However, we attach a great importance to the use of technique of inkjet printing the seeding layer as a simple, feasible, and effective approach.

In this work, the proposed technology sequence is developed and tested using industrial-type piezoresistive silicon pressure sensor devices. Despite other pressure sensor concepts making use of piezoelectric, capacitive, optical, SAW, or resonance approaches, the piezoresistive pressure sensors are by far the mostly used one in numerous approaches. Hence, this sensor type was chosen for our investigations.

2. Experimental Section

2.1. Piezoresistive Pressure Sensor Device

Industrial-type silicon-based piezoresistive pressure sensor devices fabricate on 4-inch silicon wafers were used, as shown in **Figure 1**. These sensors feature implanted highly B-doped sites in the high-strain regions of the diaphragm. The diaphragm was prepared by isotropic KOH etching on the rear side, resulting in the diaphragm thickness of 130 μm. This thickness is typically used for pressure measurements in the range of (0–30) bar. On the front side, a standard metallization scheme made of a photolithografically structured sputtered AlSi layer was used in a combination with a SiO_2 passivating layer. The four piezoresistors

were connected in a Wheatstone bridge to maximize the signal output. Such a design is described in detail elsewhere.[21]

2.2. Local Seeding and Low-Temperature Diamond Growth

After completion of the manufacturing of the device wafer, the passivation layer of diamond was locally applied. Necessarily, a compatible process sequence was performed, which consists of a sequence of local nanodiamond seeding and the low-temperature synthesis of a NCD layer. Especially the metallization scheme of AlSi used at the device wafer does not allow us to synthesize the diamond at a typical temperature of 600–800 °C.

First, on wafer level, a local seeding layer was applied by ink jet printing of an ink containing nanodiamonds stabilized in DMSO from ADAMAS Nanotechnologies and additional stabilizing agents. The inkjet printer used was a PixDro LP 50 system featuring a SPECTRA 128 SL printing head with 128 nozzles and a nominal volume of 80 pl. The bottom side of diaphragm was completely covered with the ink using a dot pattern with a resolution of 325 dpi having a nominal overlap of 30%. Also on the side wall of the cavity, the ink with nanodiamonds was deposited. The chuck temperature of the inkjet system was set to 60 °C to dry the solvents of the ink. In Figure 3a,b, the seeded nanodiamonds are shown in SEM images. Using such SEM pictures, the seeding density was calculated by image analysis as fraction of the seeded area compared to the complete picture area.[3]

Second, the diamond synthesis was performed on the rear side of the wafer on the seeded diaphragm. The diamond growth was performed in a linear-antenna microwave plasma-enhanced chemical vapour deposition (LA MW PE CVD) system.[9] The gas mixture of $H_2/CH_4/CO_2$ (at a ratio of 0.92:0.02:0.06) was used. The total gas pressure was 24 Pa, with the total gas flow maintained at 150 sccm. The substrate stage temperature of 290 °C was monitored by a thermocouple inside the stage. The average MW power was (1425 ± 50) W operated in a pulse mode (48.8% duty cycle and 42 kHz repetition frequency). The samples-to-antennas distance was 3.5 cm. The film thickness was monitored by in situ laser reflection interferometry, laser wavelength was 405 nm. At ≈290 °C, a NCD thin film of 540 nm thickness was grown in 65 h 40 min at rate of ≈8.2 nm h^{-1}, resulting in a uniform covering of the silicon surface. The total temperature on the wafer surface might be higher than 290 °C, but an adequate measurement technique is not available for the reactor. The diamond layer analysis was performed by scanning electron
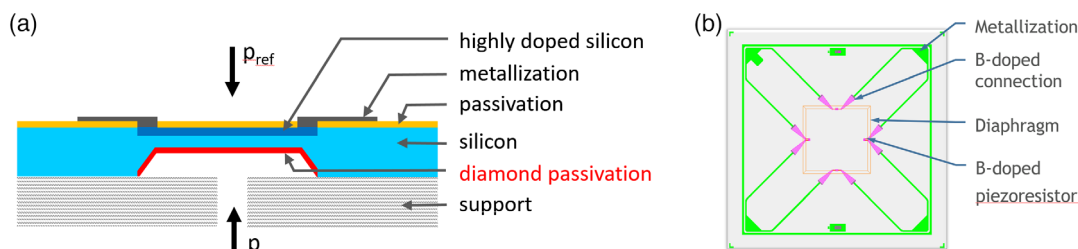
Figure 1. Drafts of the pressure sensor device developed. In a), the cross section is shown, in b) the top view from the contacts: green – AlSi metallization, pink – heavily B-doping as electrical connection to the piezoresistive sites (not visible in this magnification), yellow – position of diaphragm. The support under the silicon device is another silicon wafer, bonded to the device wafer to gain mechanical stability. A (corrosive) medium puts the pressure p at the rear side of the diaphragm, resulting in a sensor signal.

microscopy (ZEISS Auriga 60 Crossbeam) and Raman spectrometry (Horiba Jobin Yvon T64000 spectrometer in a confocal micro-Raman setup excited by an argon ion laser with a wavelength of 488 nm).

2.3. Assembly of Devices

The manufacturing process was finished by bonding the 4-inch device wafer onto the silicon support wafer (thickness 2.1 mm) by glass frit bonding, as shown in Figure 1a. This support provides the necessary stiffness to the chip. Further, this wafer stack was cut into single sensor devices of an edge length of $6.6 \times 6.6 \, mm^2$. Single sensors were implemented into a commercial TO-8 socket, by glass frit bonding the silicon chip to the TO-8 socket and wire bonding the electrical connections using a thin Au wire, as shown in **Figure 2**. Now, the diamond passivation layer is buried to the inside volume and so prevents the device wafer from chemical corrosion when the device is operated.

In parallel to the devices with additional diamond layer, also a batch of reference devices was processed, to investigate the influence of the additional diamond layer to the performance of the sensor devices.

2.4. Test of the Pressure Sensor Devices

Electrical performance was measured prior to and after diamond synthesis on wafer level for several sensor chips revealing that neither the CVD procedure nor the additional diamond layer has significant effects onto the performance indices such as bridge resistance or thermal coefficient of resistance (results not shown here). More important are the results of the single sensor devices mounted on TO-8 sockets, which were submitted to a standard test procedure including 1) measurements of the electrical performance of devices undergoing temperature (−40 to 130 °C) and pressure hysteresis curves and 2) thermal stability measurements by observing the electrical performance at a set temperature of 135 °C for 24 h.

## 3. Measurement Results

3.1. Diamond Layer

The seeding homogeneity and the diamond layer were both characterized by SEM and by Raman spectroscopy in the case of the diamond layer.

The seeding was proofed to be homogeneous all over the rear side of the diaphragm with an average particle area of less than $100 \, nm^2$. Single inkjet spots of a diameter of $\approx 130 \, \mu m$ are distinguishable with the seeding density of better than 13%, as calculated from SEM images, see **Figure 3**a–c. The smallest spots were $\approx 80 \, \mu m$ in diameter. Nevertheless, the so called coffee rings appear, indicating a slightly inhomogeneous particle size distribution due to drying effects of the jetted spots (Figure 3d). The SEM images also reveal the nanocrystalline morphology of the diamond layer (Figure 3e,f). In FIB-prepared cross sections, the thickness of the diamond layer was measured in the range of 450–500 nm (Figure 3g). The diamond synthesis uniformity on elevated structures and in the 300 μm deep cavities with the inclined side walls was homogeneous (Figure 3h).

The Raman spectroscopy reveals clearly the diamond features, in the following given as wavelength shift relative to the excitation wavelength of 488 nm: The sp^3-related diamond peak at relative wavelength shifts of $1334 \, cm^{-1}$ can be clearly determined, see **Figure 4**.

The baseline correction and the Lorentzian fit to the centered diamond peak (at a position of $1334.0 \, cm^{-1}$ and $FWHM = 17.5 \, cm^{-1}$) give clear evidence to the high diamond quality of the deposited layer. Both sp2-related peaks, the D-Band at $1320 \, cm^{-1}$ and G-Band at $1569 \, cm^{-1}$, can be clearly determined, see Figure 4. Additional features at 1154 and $1490 \, cm^{-1}$ are assigned to transpolyacetylene (TPA).[22]

Lorentz curve fitting was applied to the diamond and non-diamond related peaks at $1334 \, cm^{-1}$, and at 1154, 1320, 1490, and $1569 \, cm^{-1}$. Applying the formula given by Fortunato et al., a high sp^3 content of 95% is calculated, making use of the areas under the individual curves.[23]
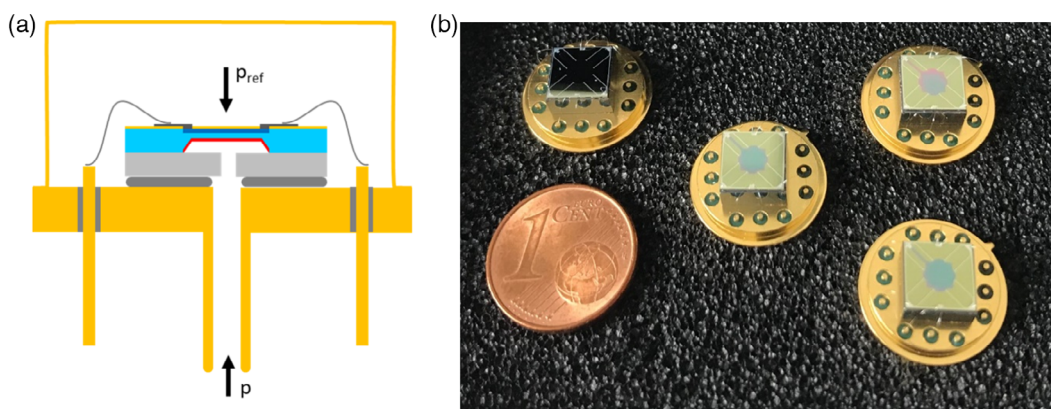

Figure 2. a) Schematic of the pressure sensor device mounted to a TO-8 header by glass frit bonding and electrically connected via wire bonding (not to scale) and with housing. The rear side is pneumatically connected to the pressure to be measured. A (corrosive) medium puts the pressure p to the rear of the diaphragm, resulting in a sensor signal. The sensor device diaphragm is the most fragile element, which is prevented from chemical corrosion by the additional diamond layer. b) A set of prepared sensor devices, compared to a 1 €ct coin. The diameter of the TO-8 header is 12.7 mm, the pressure sensor side length is 6.6 mm.
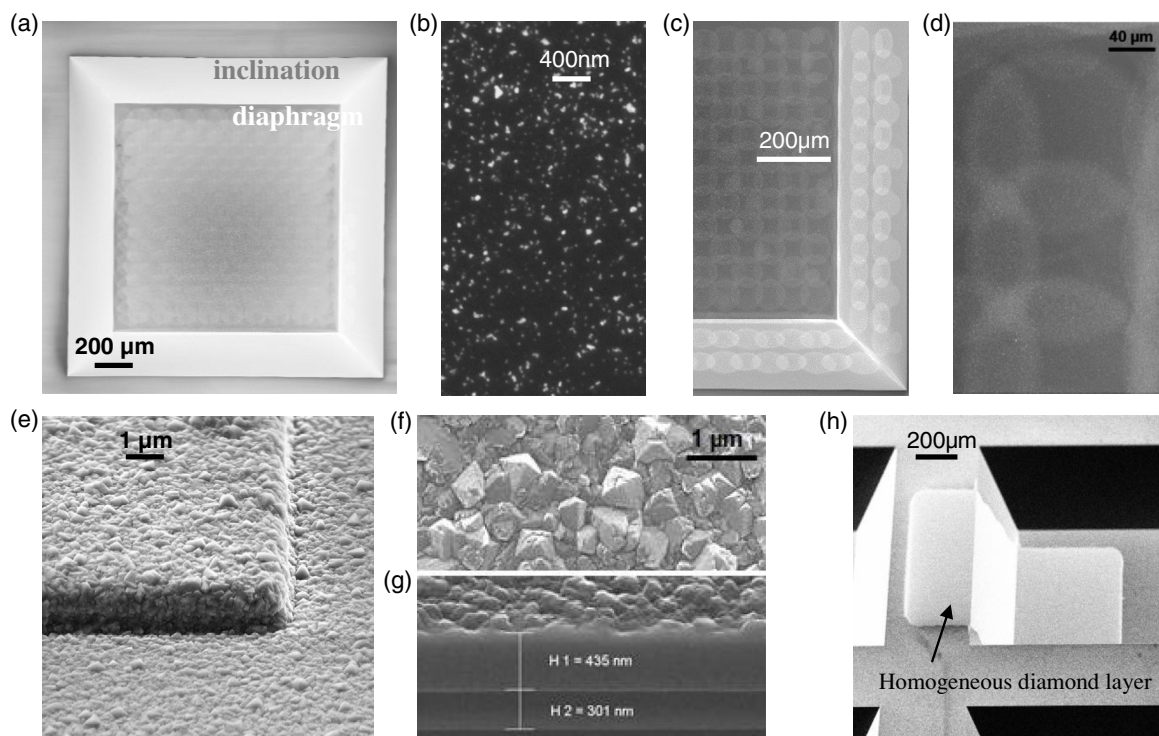
Figure 3. SEM investigations: a) view of the rear side of the silicon wafer with centrally arranged squared diaphragm was the visble nanodiamond seeded layer. b) The rear side of silicon diaphragm after inkjet seeding and drying: bright spots reveal a homogeneous density of diamond nanocrystals. c) A continuous seeding can be achieved also on the 54.7° inclination side of the diaphragm including corners. d) Overlapping of individual inkjet spots: brighter areas correlate with a slightly higher nanocrystal density. The so-called coffee ring effect is a slightly increased density of diamond nanocrystals at the edge of individual inkjet spots due to drying effects. Picture 3b) was taken in the area without overlaps and coffee rings. e) 3d-conform deposition of the NCD layer on a test structure. f) Top view onto the diamond layer. g) FIB-prepared cross section showing the diamond layer (435 nm) on a Si test wafer with SiO_2 coating (301 nm). h) Test structure with seeding and subsequent diamond synthesis into a 300 μm deep cavity in Si.
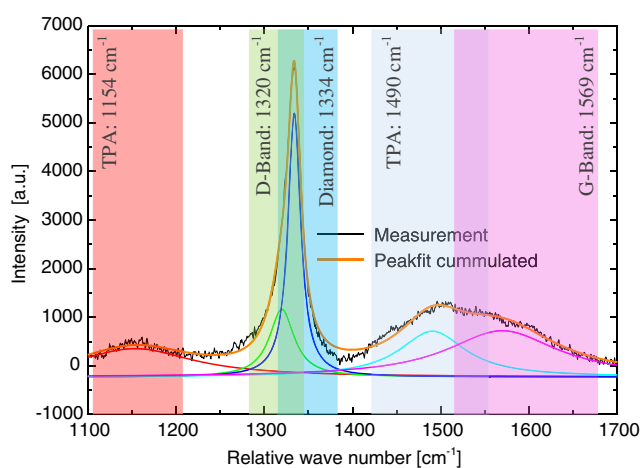
Figure 4. Raman spectra on a test structure: The Lorentz curve fitted to the relevant peak is shown.

3.2. Single Sensor Chips

A batch of three sensor chips with and four without diamond layer mounted on TO-8 sockets were tested by applying an industry-typical test regime, but only two representative sets of measurements are shown discussed in this paper. The so-called pressure–temperature hysteresis measurements were made (**Figure 5**). The sensitivity represents the sensor bridge signal, taken at normal pressure. A typical decrease in the sensitivity from 23 to 15 mV V^{-1} for increased temperatures from −40 to 130 °C is obtained for both sensors. The sensitivity of the diamond coated sensor devices has decreased by only 1 mV V^{-1} as compared to the uncoated devices revealing the influence of the diamond layer. This is explained by the increased stiffness of the silicon diaphragm with the diamond layer, which was expected and correlates in general very well with the finite element simulations performed using COMSOL (results are not shown here).

The pressure curves indicate a direct correlation of the output voltage versus applied pressure in the range of 0 to 25 bar, which is almost identical for both sensor devices with and without diamond layer. Here, the nonlinearity calculated by the endpoint method shows also a typical trend with a maximum value of 0.2% full scale for both sensors.

The zero-point stability characterizes the mechanical stability of the sensor system, mainly the assembly and migration effects. If the zero point is drifting at increased temperatures over several hours, e.g., the bonding quality of the assembly must be optimized. The measurement is for both sensors with and without
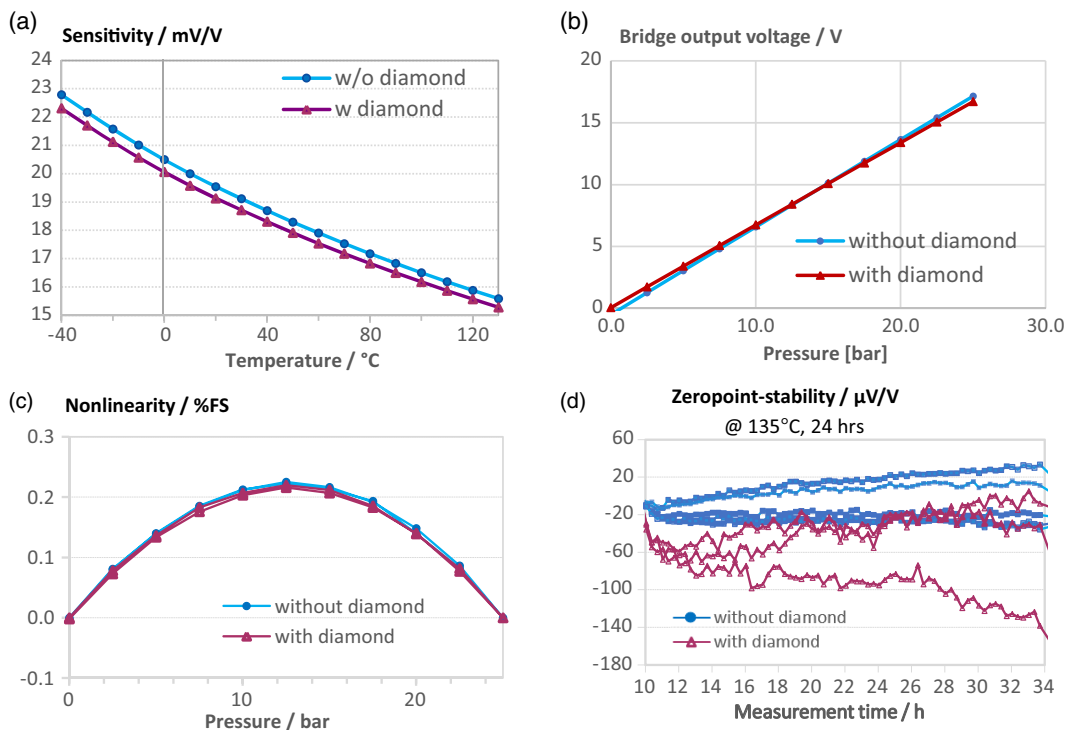
Figure 5. Results of the pressure sensor characterization. a) Sensitivity versus temperature. b) Bridge output voltage versus pressure at 30 °C. c) Nonlinearity versus pressure at 30 °C and d) the long time stability characterized by zero-point stability for 24 h at 135 °C.

diamond in a good range of -140 to $+20\,\mu V\,V^{-1}$ revealing a high stability of the device, especially of the bonding interfaces. However, an impact of the diamond layer on the zero-point stability was not expected, either.

4. Discussion

The quality of the local seeding by inkjet spotting was good with an diameter of typically 130 µm. Smallest spots of a diameter of ≈80 µm were observed. The spot size can be further reduced by means of a small-volume printing head. The locally proofed seeding proportion was 13 %. Nevertheless, the visible coffee ring effects can be optimized, also in combination with the visible overlap areas. Adjusting these homogeneities will most probably leads to a higher homogeneity of the grown diamond layer for even smaller thicknesses than 500 nm. For the layer thickness tested in this paper, no detrimental effect could be determined. The high quality of the diamond film was proofed by Raman measurements revealing a sp^3 content of 95%, pointing out the high quality of the NCD film, despite the low substrate temperature of ≈290 °C. Also the thickness homogeneity of the diamond film especially on 3*d*-structures was very good.

Since the test results of the pressure sensor devices with a diamond film were absolutely comparable to those without, a very good process compatibility of the proofed process sequence for applying the diamond layer to the CMOS-based processing of the pressure sensor chip was achieved.

5. Conclusion

The preparation of pressure sensor devices with an additional diamond passivation coating was successfully demonstrated by means of inkjet printing locally, the nanodiamond seeding layer on the rear side of the pressure sensor diaphragm, and low-temperature diamond growth in a linear antenna MW PE CVD reactor at <300 °C. Only at the seeded sites, the synthesis of a high-quality diamond film was done without any unintended diamond growth on not seeded sites. The lateral resolution was limited to 80 µm; nevertheless, it can be further reduced by using other inkjet printing heads with smaller drop volumes.

Remarkably, this diamond passivation layer was applied in a backend process on wafer level: diamond CVD temperatures were compatible to the already processed sensor device and an additional structuring of the diamond layer was not necessary, which demonstrates the simplicity of our approach. Standard testing results revealed that the diamond layer does not hamper the stability of the device assembled to a support wafer and further to a TO-8 socket. It also does not affect the pressure sensor performance as compared to sensor devices without diamond layer.

This proofed method of postprocessing and only local and low-temperature synthesis of a diamond layer suggests many other applications, heading for chemical inertness and mechanically stability of sensor devices, e.g., on AFM tips or interdigitated electrodes. Another degree of freedom is the conductance of the diamond coating that can be engineered. The potential of this method is high since the diamond layer was applied by only two

additional process steps that were performed on a wafer level: the inkjet seeding is an already industrialized process with the capability of processing several hundreds of wafers per hour, and the linear antenna microwave plasma-enhanced chemical vapor deposition reactors are known from the photovoltaic industries with very high throughput. In general, this makes the approach cost effective and very attractive.

Conflict of Interest

The authors declare no conflict of interest.

Data Availability Statement

The data that support the findings of this study are available from the corresponding author upon reasonable request.

[1] H. Sharifi, R. R. Lahiji, H.-C. Lin, D. Y. Peide, L. P. Katehi, S. Mohammadi, *IEEE Trans. Adv. Packag.* **2009**, *32*, 84.

[2] A. A. Barlian, R. Narain, J. T. Li, C. E. Quance, A. C. Ho, V. Mukundan, B. L. Pruitt, 19th IEEE Int. Conf. on Micro Electro Mechanical Systems, IEEE, Piscataway, NJ **2006**, pp. 626–629, https://doi.org/10.1109/MEMSYS.2006.1627877.

[3] H. J. Fecht, K. Brühne, *Carbon-Based Nanomaterials and Hybrids: Synthesis, Properties, and Commercial Applications*, CRC Press **2014**, ch 7.

[4] A. F. Sartori, P. Belardinelli, R. J. Dolleman, P. G. Steeneken, M. K. Ghatkesar, J. G. Buijnsters, *Small* **2019**, *15*, 1803774.

[5] J. Zalieckas, I. R. Mondragon, P. Pobedinskas, A. S. Kristoffersen, S. Mohamed-Ahmed, C. Gjerde, P. J. Høl, G. Hallan, O. N. Furnes, M.-R. Cimpan, K. Haenen, B. Holst, M. M. Greve, Polycrystalline Diamond Coating on Orthopaedic Implants: Realization, and Role of Surface Topology and Chemistry in Adsorption of Proteins and Cell Proliferation, **2022**.

[6] M. Cramer, I. Verboven, J. Drijkoningen, W. Deferme, in *Organic Electronics and Photonics: Fundamentals and Devices*, SPIE Photonics Europe, Strasbourg, France, May **2018**, vol. *10687*, pp. 11. https://doi.org/10.1117/12.2306084.

[7] D. Mukherjee, F. Oliveira, S. Camargo Trippe, S. Rotter, M. Neto, R. Silva, A. K. Mallik, K. Haenen, C.-M. Zetterling, J. C. Mendes, *Diamond Relat. Mater.* **2020**, *101*, 107625.

[8] B. Baudrillart, F. Bénédic, Th Chauveau, A. Bartholomot, J. Achard, *Diamond Relat. Mater.* **2017**, *75*, 44.

[9] S. Drijkoningen, P. Pobedinskas, S. Korneychuk, A. Momot, Y. Balasubramaniam, M. K. Van Bael, S. Turner, J. Verbeeck, M. Nesládek, K. Haenen, *Cryst. Growth Des.* **2017**, *17*, 4306.

[10] J. Zalieckas, P. Pobedinskas, M. M. Greve, K. Eikehaug, K. Haenen, B. Holst, *Diamond Relat. Mater.* **2021**, *116*, 108394.

[11] N. Wiora, M. Mertens, M. Mohr, K. Brühne, H.-J. Fecht, *Diamond Relat. Mater.* **2016**, *70*, 145.

[12] A. Yamamoto, N. Nawachi, T. Tsutsumoto, H. Nishiie, T. Asahi, *New Diamond Front. Carbon Technol.* **2005**, *15*, 1.

[13] S. D. Janssens, S. Drijkoningen, K. Haenen, *Appl. Phys. Lett.* **2014**, *104*, 073107.

[14] S. Drijkoningen, S. D. Janssens, P. Pobedinskas, S. Koizumi, M. K. Van Bael, K. Haenen, *Sci. Rep.* **2016**, *6*, 35667.

[15] M. Adamschik, R. Müller, P. Gluche, A. Flöter, W. Limmer, R. Sauer, E. Kohn, *Diamond Relat. Mater.* **2001**, *10*, 1670.

[16] G. M. Swain, *J. Electrochem. Soc.* **1994**, *141*, 3382.

[17] N. Yang, S. Yu, J. V. Macpherson, Y. Einaga, H. Zhao, G. Zhao, G. M. Swain, X. Jiang, *Chem. Soc. Rev.* **2018**, *48*, 157.

[18] H. Zhao, G. Wei, J. Gao, Z. Liu, G. Zhao, *ChemElectroChem* **2015**, *2*, 366.

[19] A. Bongrain, E. Scorsone, L. Rousseau, G. Lissorgues, C. Gesset, S. Saada, P. Bergonzo, *J. Micromech. Microeng.* **2009**, *19* 074015.

[20] *Nanodiamond* (Ed: O. A. Williams), Royal Society of Chemistry, Cambridge **2014**, Ch. 10—Diamond Nucleation and Seeding Techniques.

[21] H. Ngo, P. Mackowiack, N. Grabbert, T. Weiland, X. Hu, M. Schneider-Ramelow, O. Ehrmann, K.-D. Lang, in *2017 Eleventh Int. Conf. on Sensing Technology (ICST)*, Sydney, NSW, Australia, December **2017**, pp. 1–6, https://doi.org/10.1109/ICSensT.2017.8304457.

[22] S. Prawer, R. J. Nemanich, *Philos. Trans. R. Soc. A: Math. Phys. Eng. Sci.* **2004**, *362*, 2537.

[23] W. Fortunato, A. J. Chiquito, J. C. Galzerani, J. R. Moro, *J. Mater. Sci.* **2007**, *42* 7331.